Determinants and Characteristics of Bruch's Membrane Opening and Bruch's Membrane Opening–Minimum Rim Width in a Normal Japanese Population

Makoto Araie,[1] Aiko Iwase,[2] Kazuhisa Sugiyama,[3] Toru Nakazawa,[4] Goji Tomita,[5] Masanori Hangai,[6] Yasuo Yanagi,[7] Hiroshi Murata,[7] Hidenobu Tanihara,[8] Claude F. Burgoyne,[9] and Balwantray C. Chauhan[10]

[1]Kanto Central Hospital of the Mutual Aid Association of Public School Teachers, Tokyo, Japan
[2]Tajimi Iwase Eye Clinic, Tajimi, Japan
[3]Department of Ophthalmology and Visual Science, Kanazawa University Graduate School of Medical Science, Kanazawa, Japan
[4]Department of Ophthalmology, Tohoku University Graduate School of Medicine, Sendai, Japan
[5]Department of Ophthalmology, Toho University Ohashi Medical Center, Tokyo, Japan
[6]Department of Ophthalmology, Saitama Medical School, Moro, Japan
[7]Department of Ophthalmology, The University of Tokyo Graduate School of Medicine, Tokyo, Japan
[8]Department of Ophthalmology, Faculty of Life Sciences, Kumamoto University, Kumamoto, Japan
[9]Devers Eye Institute, Portland, Oregon, United States
[10]Department of Ophthalmology and Visual Science, Dalhousie University, Halifax, Nova Scotia, Canada

Correspondence: Makoto Araie, Kanto Central Hospital of the Mutual Aid Association of Public School Teachers, 6-25-1, Kamiyoga Setagaya-ku, Tokyo, 158-8531, Japan; araie-tky@umin.net.

Submitted: April 18, 2017
Accepted: July 18, 2017

Citation: Araie M, Iwase A, Sugiyama K, et al. Determinants and characteristics of Bruch's membrane opening and Bruch's membrane opening–minimum rim width in a normal Japanese population. *Invest Ophthalmol Vis Sci*. 2017;58:4106–4113. DOI: 10.1167/iovs.17-22057

Purpose. To identify determinants of Bruch's membrane opening (BMO), and BMO–minimum rim width (BMO-MRW) and circumpapillary retinal nerve fiber layer thickness (RNFLT) centered on BMO center and characterize these parameters in a normal Japanese population.

Methods. Spectral-domain optical coherence tomography images of optic nerve head and circumpapillary and macular retina were obtained in 258 eyes of 258 normal Japanese with mean (standard deviation) age of 51.7 (18.2) years. BMO area, BMO-MRW, RNFLT (measured with a 3.5-mm-diameter circle scan) were all acquired and analyzed relative to the eye-specific fovea to BMO (FoBMO) axis. One randomly selected eye of each subject was analyzed. Multiple regression analysis was used to identify determinants to the parameters.

Results. BMO area, global BMO-MRW, RNFLT, and FoBMO angle averaged 2.06 (0.45) mm^2, 305.5 (50.0) μm, 101.8 (9.6) μm, and −7.8° (3.8°), respectively. There was a modest correlation between global BMO-MRW and RNFLT ($r = 0.337$; $P < 0.001$), while the sectorwise correlations were highest in the superior-temporal sector ($r = 0.500$; $P < 0.001$) and lowest in the nasal sector ($r = 0.117$; $P = 0.063$). Global BMO-MRW and RNFLT declined with age at −1.04 μm/y ($P < 0.001$) and −0.12 μm/y ($P = 0.001$), and the former correlated negatively ($P = 0.001$) and the latter positively ($P < 0.001$) with BMO area after adjustment for other factors ($R^2 = 0.191$ and 0.272, respectively). BMO area correlated positively with axial length ($P = 0.023$) and negatively with age ($P < 0.001$) ($R^2 = 0.157$).

Conclusions. BMO-MRW and RNFLT declined with age with a difference between them in their relationship to BMO area. BMO area positively correlated with axial length and negatively with age.

Keywords: Bruch's membrane opening, minimum rim width, optical coherence tomography

Glaucoma is a progressive disease of the optic nerve head (ONH) and retinal nerve fiber layer (RNFL) with characteristic change in the neuroretinal rim identified by conventional clinical fundus examination.[1] Recent advances in spectral-domain optical coherence tomography (SD-OCT) technology has allowed imaging of the neuroretinal rim and the RNFL, as well as more detailed ONH structures such as the lamina cribrosa and termination of Bruch's membrane–retinal pigment epithelium complex.[2–8]

Recently, Bruch's membrane opening (BMO) has been proposed as a new anatomically identifiable aperture through which retinal ganglion cell (RGC) axons leave the eye.[9] The minimum rim width from BMO, termed "Bruch's membrane opening–minimum rim width" (BMO-MRW), is the minimum distance between BMO and the internal limiting membrane, and thought to be anatomically and geometrically more accurate than conventional clinical disc margin–based rim parameters.[9] Recently in independent studies, BMO-MRW has been reported to have higher correlation with visual field damage and higher diagnostic accuracy for glaucoma than conventional disc margin–based neuroretinal rim parameters.[10–13] It has also been proposed that OCT data acquisition

and analyses be performed according to the individual eye-specific axis between the fovea and BMO center (FoBMO axis) to standardize image acquisition such that normative databases can be more accurate.[9]

Race-related differences have been reported in the conventional clinical disc and rim morphology and circumpapillary retinal nerve fiber layer thickness (RNFLT).[14–19] For example, black populations generally have greater disc size and smaller ratio of rim area to disc area than white populations,[14–16,19] and Indian and Hispanic populations have thicker circumpapillary RNFLT than white populations.[18] Further, association of the optic disc parameters with early glaucomatous damage is reportedly less apparent in black subjects than in white subjects.[17] On the other hand, characterization of BMO-MRW in healthy, nonglaucoma subjects has been reported only for a white and Chinese population,[20,21] and that of BMO and FoBMO axis for a white population only.[20] Although the clinical disc and rim area, and RNFLT in healthy, nonglaucoma subjects show significant correlation with several systemic and ocular factors, including putative risk factors for glaucoma such as age, refraction or axial length, intraocular pressure (IOP), and central corneal thickness (CCT),[18,19,22–36] no such correlations have been studied in detail for BMO or BMO-MRW.

The objectives of the current study were to (1) examine whether previously reported ocular and systemic factors that correlate with conventional clinical disc and rim area[18,19,22,30,32–34] or OCT-measured RNFLT and macular RGC layer thicknesses[18,19,31,35–39] also impact the BMO, BMO-MRW, and FoBMO angle and (2) report characteristics of these parameters, based on BMO, in a normal Japanese population.

Subjects and Methods

Subjects

Approximately the same number of self-reported generally healthy Japanese subjects in each of six age groups by decade was recruited at seven Japanese clinical centers: University of Tokyo Hospital (Tokyo, Japan), Toho University Ohashi Medical Center (Tokyo, Japan), Tajimi Eye Clinic (Tajimi, Japan), Saitama Medical School Hospital (Moro, Japan), Tohoku University Hospital (Sendai, Japan), Kumamoto University Hospital (Kumamoto, Japan), and Kanazawa University Hospital (Kanazawa Japan).

After verbal screening of participation and questioning of medical history, an ocular examination including uncorrected and autorefraction-corrected visual acuity measurements with the 5 m-Landolt chart, corneal curvature measurements, and axial length measurement (IOLMaster; Carl Zeiss Meditec, Dublin, CA, USA) was performed. Thereafter, the visual field was examined with standard automated perimetry (Humphrey Field Analyzer; Carl Zeiss Meditec) with the 24-2 Swedish Interactive Thresholding Algorithm. The visual field examination was repeated if not deemed reliable or within normal limits. The OCT examination (see below) was then performed, followed by dilated funduscopy, optic disc stereophotography, slit lamp biomicroscopy, IOP measurements with the Goldmann applanation tonometer, and optical pachymetry to measure CCT. All ocular examinations were done bilaterally.

Inclusion criteria were (1) age between 20 and 90 years; (2) normal eye examination results without clinically significant cataract, vitreoretinal, or choroidal abnormalities (subjects with uncomplicated cataract surgery were not excluded); (3) IOP $\leq$ 21 mm Hg; (4) best corrected visual acuity $\geq$ 20/40; (5) spherical error $\leq \pm 6$ diopters (D) and astigmatism $\leq$ 2 D; (6) axial length $\leq$ 26 mm; and (7) normal visual field test results with the glaucoma hemifield test and mean deviation within normal limits. Subjects were excluded if (1) the visual field results were deemed unreliable with the perimetrist's notes and reliability indices; (2) the optic disc stereophotographs were of insufficient quality; or (3) the OCT images were of insufficient quality (typically truncated B-scans and scans with image quality score of $<$20).

The Institutional Review Board and Ethics Committee of each participating center approved the study, which adhered to the tenets of the Declaration of Helsinki. Written informed consent was obtained from each subject after full explanation of the protocol.

Spectral-Domain Optical Coherence Tomography

The ONH, peripapillary RNFL, and macula were imaged with OCT (Spectralis, Glaucoma Module Premium Edition; Heidelberg Engineering GmbH, Heidelberg, Germany). For the ONH, the foveal pit and two BMO points in each of two radial B-scans that were perpendicular to each other were automatically segmented to estimate the center of BMO and determine the FoBMO axis, which served as a reference for all scans. A scan containing 24 radially equidistant B-scans, each subtending 7.5°, centered on BMO, was then acquired. Each radial B-scan contained 1536 A-scans, averaged 25 times. ONH scans were determined with standard and enhanced depth imaging modes.[40] For the RNFLT measurements, circular peripapillary scans with 768 A-scans, each representing the average of 100 individual scans, were obtained with circles subtending 12°, 14°, and 16° and also diameters measuring 3.5, 4.1, and 4.7 mm centered on the BMO center to measure the RNFLT. Axial length and corneal curvature measurements were entered into the instrument software to ensure accurate scaling of all measurements. In this report, only the results from the standard ONH radial B-scans and the 3.5-mm-diameter RNFLT scans centered on BMO center were analyzed.

All eyes were converted to right-eye format. The software automatically segmented the internal limiting membrane and the 48 BMO points from the 24 radial scans. The segmentation was manually checked in each B-scan and corrected when necessary. The BMO points were fitted with a spline to derive a closed curve to represent the BMO around the ONH. BMO torsion was measured by the parameter *BMO torsion angle*, which was defined to be the angle between the longest axis of BMO (the radial B-scan with the longest BMO length) and the FoBMO vertical axis (the axis passing through the BMO center, perpendicular to the FoBMO axis).[20] The *FoBMO angle* was defined to be the angle between the FoBMO axis and the horizontal axis of the acquired image frame (Fig. 1).[9,20] The global and the six Garway-Heath regional BMO-MRW and RNFLT values (40° superonasal [SN], 40° inferonasal [IN], 40° inferotemporal [IT], 40° superotemporal [ST], 90° temporal [T], and 110° nasal [N] sectoral values)[41] were calculated. For each subject, all orientations were relative to the FoBMO axis.

Data Analysis

Results were presented as mean (standard deviation). Correlation among variables was computed with Pearson's correlation coefficients when variables were parametric and generally conformed to the normal distribution, or Spearman's correlation coefficients when variables were nonparametric or apparently did not conform to the normal distribution. The influence of systemic and ocular factors on global BMO-MRW,

Investigative Ophthalmology & Visual Science

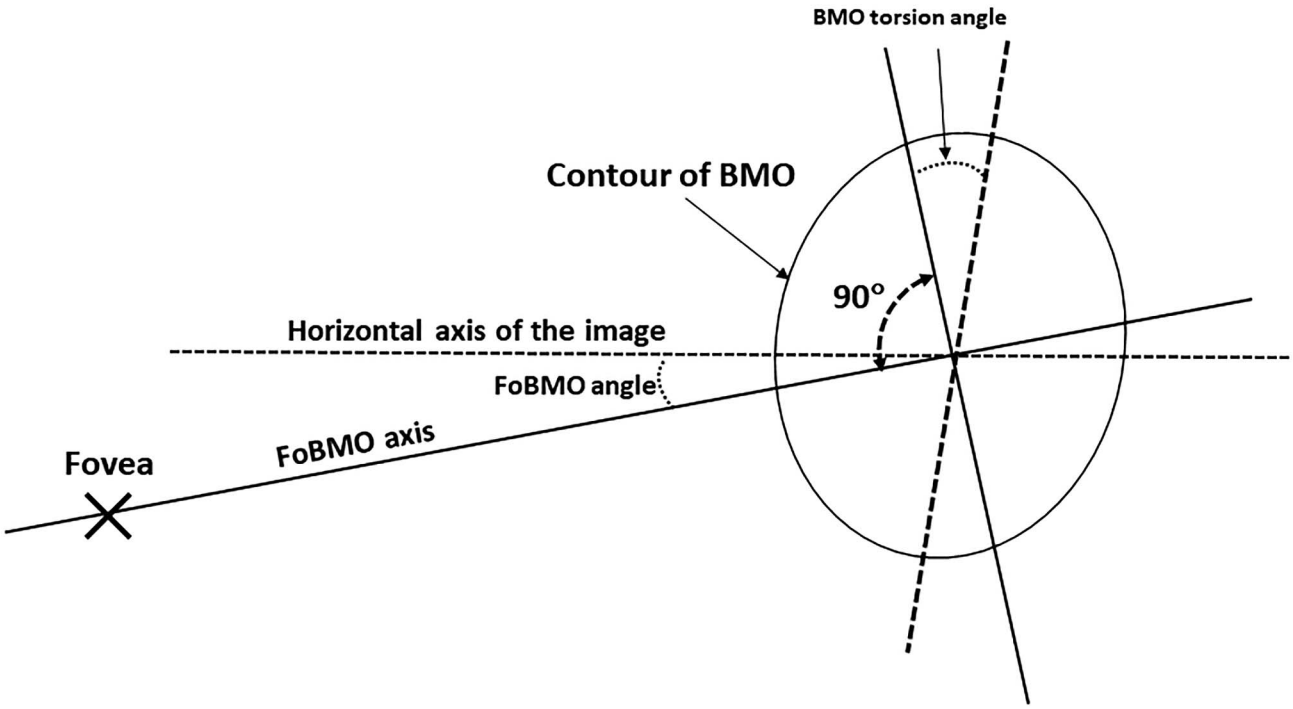

Figure 1. Diagram illustrating *FoBMO angle* and *BMO torsion angle*. FoBMO axis, fovea and BMO center axis; *FoBMO angle*, angle of FoBMO axis relative to the horizontal axis of the image; and *BMO torsion angle*, the orientation of the long axis of BMO (*broken line*) relative to the axis perpendicular to the FoBMO axis. A positive (negative) *FoBMO angle* indicates the fovea located above (below) the horizontal line passing through BMO center, and a positive (negative) *BMO torsion angle* value indicates inferotemporal (superonasal) torsion relative to the axis perpendicular to the FoBMO axis.

RNFLT, BMO area, *FoBMO angle*, and *BMO torsion angle* were analyzed with multiple regression analysis.

For global BMO-MRW and RNFL, factors previously shown to be associated with clinical disc margin–based rim area and RNFLT in normal eyes, namely, age, disc area, CCT, IOP, axial length or refractive error, and sex,[19–23,26–27,30–39] were tested as explanatory variables. Similarly, as sex, age, refraction, axial length, rim area, and RNFLT[14,19,22,24–30,32,36] have been reported to be correlated to clinical disc margin–based disc area, these variables were tested as explanatory variables for OCT BMO area. Previous studies measuring the location of fovea relative to the optic disc in fundus photographs suggest a possible intereye difference in the extent of excyclotorsion[42–44] and age-dependence of *FoBMO angle*[45] in normal subjects. We therefore explored whether similar relationships were present within our subjects for the parameters *FoBMO angle* and *BMO torsion angle*.

Table 1. Summary of Subjects' Characteristics

Parameter	Mean (Standard Deviation)	Range
No. of subjects, eyes	258 (258)	
Sex, male/female	128/130	
Eye, right/left	129/129	
Age, y	51.7 (18.2)	20.3 ~ 88.8
Axial length, mm	23.9 (1.0)	21.3 ~ 26.0
Spherical equivalent refraction, D	−0.6 (1.8)	−6.5 ~ 4.8
Intraocular pressure, mm Hg	14.0 (2.3)	8 ~ 19
Central corneal thickness, μm	538 (35)	453 ~ 666

Sectoral values of BMO-MRW and RNFLT were also analyzed with liner mixed effects modeling (LMM), taking the intersectoral correlation of BMW-MRW and of RNFLT into consideration.

Data analyses were performed with SPSS (21.0J for Windows; SPSS Japan, Inc., Tokyo, Japan). LMM analyses were performed with the statistical programming language R (R version 3.1.3; Foundation for Statistical Computing, Vienna, Austria).

Results

For analysis of BMO area, BMO-MRW, *FoBMO angle*, and *BMO torsion angle*, 258 eyes of 258 subjects satisfied the inclusion and exclusion criteria (Table 1). The number of subjects in each decade group was between 35 and 45 except for the group older than 80 years (Fig. 2). The respective number for the analysis of RNFLT was 243 eyes of 243 subjects (Table 1), since 15 eyes yielding reliable BMO-MRW measurement results did not yield reliable RNFLT measurements results.

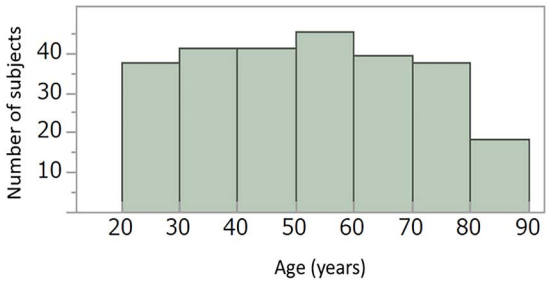

Figure 2. Age distribution of the current subjects.

Table 2. Results of Optical Coherence Tomography Measurements

Parameters	Mean (Standard Deviation)
BMO area, mm^2	2.06 (0.45)
The longest diameter of BMO, mm	1.75 (0.19)
The shortest diameter of BMO, mm	1.49 (0.17)
Global BMO-MRW, μm	305.5 (50.0)
BMO-MRW-T, μm	220.0 (40.4)
BMO-MRW-ST, μm	298.1 (53.1)
BMO-MRW-IT, μm	336.3 (53.7)
BMO-MRW-N, μm	329.0 (67.6)
BMO-MRW-SN, μm	346.7 (63.7)
BMO-MRW-IN, μm	368.7 (63.7)
Global RNFLT, μm*	101.8 (9.6)
RNFLT-T, μm*	76.0 (10.9)
RNFLT-ST, μm*	133.7 (21.0)
RNFLT-IT, μm*	156.3 (18.7)
RNFLT-N, μm*	79.6 (12.2)
RNFLT-SN, μm*	123.1 (26.9)
RNFLT-IN, μm*	114.3 (19.8)
FoBMO angle, deg	−7.8 (3.8)
Torsion angle of BMO, deg	−13 (31)

Data are mean (standard deviation). RNFLT is measured along a circle with 3.5-mm diameter centered on BMO center. A positive (negative) *FoBMO angle* indicates the fovea located above (below) horizontal line passing through BMO center. A positive (negative) torsion angle value indicates inferotemporal (superonasal) torsion relative to the axis perpendicular to the FoBMO axis. BMO-MRW-T, -ST, -IT, -N, -SN, -IN (RNFLT-T, -ST, -IT, -N, -SN, -IN), sectoral BMO-MRW (RNFLT) values for the temporal, superotemporal, inferotemporal, nasal, superonasal, and inferotemporal sectors, respectively; *FoBMO angle*, angle of fovea-to-BMO-center axis relative to the horizontal axis of the image frame; *torsion angle* of BMO, the orientation of the long axis of BMO relative to the axis perpendicular to the FoBMO axis.

* $N = 243$.

The results of the OCT measurements are summarized in Table 2. The mean (SD) BMO area was 2.06 (0.45) mm^2. BMO shape was most commonly ovoid, with the long axis of BMO most commonly falling 13° nasally to the FoBMO vertical. Global BMO-MRW and RNFLT averaged 305.5 (50.0) μm and 101.8 (9.6) μm, respectively, while the *FoBMO angle* was −7.8° (3.8°), respectively (Table 2). Sectoral BMO-MRW was thickest in the inferior-nasal sector followed by superior-nasal and inferior-temporal sectors, while sectoral RNFLT was thickest in the inferior-temporal sector followed by superior-temporal and superior-nasal sectors (Table 2). Intersector difference in BMO-MRW or RNFLT was significant after Bonferroni's correction ($P = 0.012 \sim <0.001$) except for the difference between the IT and N and the IT and SN BMO-MRW sectoral values.

Rank order of the six sectors (T, ST, IT, N, SN, and IN sectors) showed a high degree of spatial similarity (Spearman's correlation coefficient = 0.868) in the sectoral BMO-MRW and RNFLT values. Pearson's correlation coefficients between sectoral BMO-MRW and RNFLT values were 0.337 (global), 0.187 (T), 0.340 (ST), 0.500 (IT), 0.117 (N), 0.437 (SN), and 0.348 (IN). These correlations were modest, but highly significant ($P < 0.001$), except for the T ($r = 0.187$, $P = 0.003$) and N ($r = 0.117$, $P = 0.063$) sectors where the correlations did not achieve highly statistical significance.

Among the available ocular biometric factors, corneal curvature, spherical equivalent refraction, and axial length demonstrated high interparameter correlation (all comparisons, $r > 0.650$). Thus, corneal curvature and spherical equivalent refraction were excluded from explanatory variables for multiple regression analysis, and axial length was adopted on their behalf. Multiple regression analysis showed that global BMO-MRW decreased with increasing age (−1.04 μm/y or 3.4%/decade) and BMO area (Table 3). Global RNFLT decreased with increasing age (−0.12 μm/y or 1.2%/decade) and CCT, and increased with BMO area and sex (female). BMO area increased with axial length and decreased with age and global BMO-MRW. Finally, *FoBMO angle* was more negative with age and in left eyes. No factors investigated influenced *BMO torsion angle*.

Table 3. Results of Multiple Regression Analysis

Dependent Variable	Explanatory Variable	Partial Regression Coefficient	*P* Value
Global BMO-MRW, μm	Age	−1.04 ± 0.17*	<0.001
	BMO area	−33.8 ± 6.5	0.001
Global RNFLT, μm	Age	−0.12 ± 0.04†	0.001
	BMO area	8.15 ± 1.36	<0.001
	Sex, female	2.72 ± 1.28	0.035
	CCT	−0.039 ± 0.017	0.024
BMO area, mm^2	Axial length	0.070 ± 0.031	0.023
	Age	−0.006 ± 0.002	<0.001
	Global BMO-MRW	−0.003 ± 0.001	<0.001
FoBMO angle, deg	Age	−0.041 ± 0.012	0.001
	Laterality, left	−2.36 ± 0.45	<0.001

RNFLT is measured along a circle with 3.5-mm-diameter centered on BMO center; CCT expressed in μm. A positive (negative) *FoBMO angle* indicates the fovea located above (below) horizontal line passing through BMO center.

* Age-related change corresponds to 3.4% ± 0.6%/decade.

† Age-related change corresponds to 1.2% ± 0.4%/decade.

Analysis with LMM (Appendix A) indicated that in all six sectors, BMO-MRW decreased with both age and BMO area but the impact of BMO was not the same among the six sectors (Appendix B). Sectorwise analysis of RNFLT indicated that age had a statistically significant impact only in SN, IT, and IN sectors (Appendix C). On the other hand, CCT and sex did not reach the significant level in any of the six sectors for either BMO-MRW or RNFLT.

Discussion

In recent years, the accuracy of disc margin–based neuroretinal rim measurements have been questioned.[9] Because BMO represents an anatomically identifiable outer edge of the rim, parameters such as BMO-MRW could be more accurate indicators of the rim width. Recognition that there are large interindividual variations in the position of the fovea relative to BMO has also driven OCT data acquisition and analysis according to the eye-specific *FoBMO angle*. This anatomic variation should affect ONH, RNFLT, and macular measurements as well as their regional distribution, but the clinical importance of these effects are not yet known.

A notably large interracial variation has been reported for conventional disc margin–based rim parameters,[14–19] and a similar interracial variation would be expected in BMO and BMO-MRW. Currently, however, normal values of BMO-MRW have been reported only for a white population and Chinese population,[20,21] and those of BMO for a white population only.[20] Constructing accurate normative database of BMO, BMO-MRW, and RNFLT, and identifying clinical factors relating to them for each racial group, would be of essential importance to help clinicians identify patients with glaucomatous damage.

Investigative Ophthalmology & Visual Science

In normal Japanese subjects, BMO area averaged 2.06 mm^2, a value greater than that in the normal white population (median 1.74 mm^2).[20] BMO was most commonly a vertical oval with the mean torsion angle of −13°. BMO area was greater with longer axial length (3.4% or 0.07 mm^2/mm of axial length), and smaller with age (−2.9% or 0.06 mm^2/decade) after adjusting for covariates. In contrast, BMO area is not correlated to axial length or age in a normal white population.[20] Conflicting results have also been reported on the correlation between clinical disc margin–based estimates of optic disc size, axial length, and refractive errors.[14,22,24,25,29,30,32] Although the true effect of axial length and aging on BMO area would be a subject of future studies including other racial groups, it does not seem unreasonable that a slight increase in the aperture through which axons exit the eye is associated with an elongation of axial length. The current cross-sectional study showing axial length and age dependency of BMO area suggests that for cross-sectional interindividual or intergroup comparisons of BMO area in Japanese subjects, adjustment for the axial length and age is necessary.

Global BMO-MRW and RNFLT averaged 306 and 102 μm, respectively, in normal Japanese population, and the former was similar to that reported in a normal Chinese population with a mean age of 55 years (306 μm)[21] but thinner than that reported in a normal white population with a similar age distribution (median 335 μm).[20] Global RNFLT was slightly thicker than that in a normal white population (median 100 μm).[20] These findings suggest interracial differences in the ratio of the amount of RGC axons to that of non-RGC cellular components in the retina. According to a rank order, the sectoral pattern of BMO-MRW and RNFLT was not identical, though the temporal sector was the thinnest in both of them. BMO-MRW was thickest in the IN sector followed by the SN sector, while RNFLT was thickest in the IT sector followed by the ST sector (Table 2). This pattern of sectoral thickness difference is also evident in a normal white population when using the BMO center for reference.[20] It must be noted, however, that the original six Garway-Heath regions used clinical disc center for reference,[41] and caution is needed in extrapolating the current findings to those obtained when using clinical disc center for reference.

Global and sectoral BMO-MRW decreased with age. A sector-dependent effect of aging on the RNFLT in the white population,[20] and also in the Japanese population (Appendix C), may indicate that age has a different regional impact on the neuronal and/or nonneuronal component of the RNFL, both of which are reflected in the RNFLT measurements. Global BMO-MRW declined by 1.04 μm/y, corresponding to approximately 3.4%/decade compared to 4.0%/decade (1.34 μm/y) in a normal white population.[20] A negative correlation between BMO-MRW and BMO area is understandable, since given the same number of axons, a greater BMO area would result in a thinner BMO-MRW. A negative correlation between BMO-MRW and clinical disc area has also been reported in a Chinese population.[21] Among the other factors studied, none had significant effects on BMO-MRW.

The age-related decrease in RNFLT is in agreement with numerous previous reports.[18–20,30,35,36] In the present study, RNFLT decreased by −0.12 μm/y, corresponding to 1.2%/decade decrease, which is apparently smaller than that of BMO-MRW (1.04 μm/y or 3.4%/decade). An apparently smaller rate of age-related decrease in RNRLT than in BMO-MRW (0.21 μm/y or 2.1%/decade versus 1.34 μm/y or 4.0%/decade) has also been seen in a normal white population.[20] This discrepancy may be at least partly explained by a difference in the ratio of non-RGC cellular components, for which aging causes different effects, rather than to RGC axons between the RNFL at 1.75-mm distance from the BMO center and the BMO margin. Although we could not find literature suggesting that aging shows differential effects between RGCs and their axons and non-RGC components of the retina or optic disc, one recent study[46] using experimental monkey glaucoma model suggests that effects of glaucomatous insults in this model might be different between RGCs and non-RGC components of the RNFL tissue. The age-related decline of RNFLT did not reach significant level in N and T sectors (Appendix C), indicating that age-dependent decline in the superior and inferior sectors was more evident than that in the temporal and nasal sectors. This finding is in line with that found in the normal white population on the whole,[20] and may be at least partly related to a difference in the proportion of non-RGC components in RNFL between superior/inferior and temporal/nasal sectors. A greater BMO area was associated with thicker RNFLT as reported for RNFLT centered on the clinical disc center and clinical disc area.[31,35,36] Since sectorwise analysis showed no significant impact of CCT and sex on RNFLT in any of the sectors, impacts of CCT and sex, if they exist, are thought to be small.

The *FoBMO angle* was more negative with age and significantly more negative in left than right eyes. Jonas et al.[45] have reported that a larger optic disc–fovea angle was associated with aging. Previous studies measuring the location of fovea relative to the disc in fundus photographs report a greater extent of excyclotorsion in the left compared to right eye of normal subjects.[42–44] Although the exact mechanism of the right–left difference or age-related change in the *FoBMO angle* is unknown, there have been suggestions that age-related change in the orbital connective tissue and/or rectus muscles may be partly responsible for the observed lateral difference in the extent of excyclotorsion.[44,47,48]

The current study had some limitations. Currently, both BMO-MRW and RNFLT estimates are determined without an algorithm, taking blood vessel trunks into consideration. Thus, measurements in the superior and inferior poles may not be sensitive enough to early glaucomatous changes, which are most likely to take place in the poles. The sector-dependent difference in the effect of age and BMO area on RNFLT sectoral values was found in only some sectors. It is possible that our study was underpowered to detect a significant effect in the remaining sectors. In fact, the sample size used for RNFLT analyses was somewhat smaller than that used for BMO-MRW analyses. However, it is likely that even if statistically significant, the effect is not likely to be highly clinically significant. Finally, it must be noted that the aging effects currently found were by a cross-sectional study design, but not by a longitudinal study design.

In summary, the current cross-sectional study indicated that BMO area was significantly and positively correlated with axial length and negatively with age. Age had significantly negative impact on BMO-MRW, RNFLT, and *FoBMO angle*, while BMO area was significantly and negatively correlated with BMO-MRW and positively with RNFLT. Significant intereye difference in *FoBMO angle* was also noted. Adjustment of the above factors will likely be needed for optimal diagnosis of glaucoma, using BMO-based OCT parameters.

Acknowledgments

Disclosure: **M. Araie**, Heidelberg Engineering (C), B&M (C), Santen (C, R), Senju (C), Kowa (C), Pfizer (C), Topcon (C), Allergan (C), Alcon (C), Aerie (C), Carl Zeiss (R), Otsuka (R), P; **A. Iwase**, Heidelberg Engineering (F), Carl Zeiss (R), Otsuka (R), Santen (R), Alcon (R), Pfizer (R), Topcon (R), Senju (R), Kowa (R), P; **K. Sugiyama**, Heidelberg Engineering (F); **T. Nakazawa**, Heidelberg Engineering (F), Santen (F), Senju (F), Alcon (F), Kowa (F), Topcon (F), Wakamoto (F), Nidek (F), Otsuka (F); **G. Tomita**, Heidelberg

Engineering (F), Santen (F, R), Senju (F, R), Alcon (F, R), Kowa (F), Pfizer (F); **M. Hangai**, Heidelberg Engineering (F); **Y. Yanagi**, Heidelberg Engineering (F); **H. Murata**, Beeline (R); **H. Tanihara**, Heidelberg Engineering (F), Japan Society for the Promotion of Science (F), Santen (R), Alcon (R), Pfizer (R); **C.F. Burgoyne**, Heidelberg Engineering (F), National Institutes of Health (F); **B.C. Chauhan**, Heidelberg Engineering (F), Dalhousie Medical Research Foundation (F), Allergan (R)

References

1. Shields MB. Optic nerve head and peripapillary retina. In: *Textbook of Glaucoma*. 3rd ed. Baltimore: Williams & Wilkins; 1992:84–125.
2. Srinivasan VJ, Adler DC, Chen Y, et al. Ultrahigh-speed optical coherence tomography for three-dimensional and en face imaging of the retina and optic nerve head. *Invest Ophthalmol Vis Sci*. 2008;49:5103–5110.
3. Strouthidis NG, Yang H, Reynaud JF, et al. Comparison of clinical and spectral domain optical coherence tomography optic disc margin anatomy. *Invest Ophthalmol Vis Sci*. 2009; 50:4709–4718.
4. Strouthidis NG, Grimm J, Williams GA, Cull CA, Wilson DJ, Burgoyne CF. A comparison of optic nerve head morphology viewed by spectral domain optical coherence tomography and by serial histology. *Invest Ophthalmol Vis Sci*. 2010;51: 1464–1474.
5. Agoumi Y, Sharpe GP, Hutchison DM, Nicolela MT, Artes PH, Chauhan BC. Laminar and prelaminar tissue displacement during intraocular elevation in glaucoma patients and healthy controls. *Ophthalmology*. 2011;118:52–59.
6. Lee EF, Kim TW, Weinreb RN, Park KH, Kim SH, Kim DM. Visualization of the lamina cribrosa using enhanced depth imaging spectral-domain optical coherence tomography. *Am J Ophthalmol*. 2011;152:87–95.
7. Park HY, Jeon SH, Park CK. Enhanced depth imaging detects lamina cribrosa thickness differences in normal tension glaucoma and primary open-angle glaucoma. *Ophthalmology*. 2012;119:10–20.
8. Reis AS, Sharpe GP, Yang H, Nicolela MT, Burgoyne CF, Chauhan BC. Optic disc margin anatomy in patients with glaucoma and normal controls with spectral domain optical coherence tomography. *Ophthalmology*. 2012;119:738–747.
9. Chauhan BC, Burgoyne CF. From clinical examination of the optic disc to clinical assessment of the optic nerve head: a paradigm change. *Am J Ophthalmol*. 2013;156:218–227.
10. Chauhan BC, O'Leary N, Almobarak FA, et al. Enhanced detection of open-angle glaucoma with an anatomically accurate optical coherence tomography-derived neuroretinal rim parameter. *Ophthalmology*. 2013;120:535–543.
11. Pollet-Villard F, Chiquet C, Romanet JP, et al. Structure-function relationships with spectral-domain optical coherence tomography retinal nerve fiber and optic nerve head measurements. *Invest Ophthalmol Vis Sci*. 2014;55:2953–2962.
12. Gardiner SK, Ren R, Yang H, et al. A method to estimate the amount of neuroretinal rim tissue in glaucoma: comparison with current methods for measuring rim area. *Am J Ophthalmol*. 2014;157:540–549.
13. Danthurebandara VM, Sharpe GP, Hutchison DM, et al. Enhanced structure-function relationship in glaucoma with anatomically and geometrically accurate neuroretinal rim measurement. *Invest Ophthalmol Vis Sci*. 2015;56:98–105.
14. Varma R, Tielsch JM, Quigley HA, et al. Race-, age-, gender-, and refractive error-related differences in the normal optic disc. *Arch Ophthalmol*. 1994;112:1068–1076.
15. Seider MI, Lee RY, Wang D, Pekmezci M, Porco TC, Lin SC. Optic disk size variability between African, Asian, White, Hispanic, and Filipino Americans using Heidelberg retinal tomography. *J Glaucoma*. 2009;18:595–600.
16. Girkin CA, McGwin G, Xie A, DeLeon-Ortega J. Differences in optic disc topography between black and white normal subjects. *Ophthalmology*. 2005;112:33–39.
17. Girkin CA, McGwin G Jr, McNeal SF, DeLeon-Ortega J. Racial differences in the association between optic disc topography and early glaucoma. *Invest Ophthalmol Vis Sci*. 2003;44: 3382–3387.
18. Girkin CA, McGwin G Jr, Sinai MJ, et al. Variation in optic nerve and macular structure with age and race with spectral-domain optical coherence tomography. *Ophthalmology*. 2011;118:2403–2408.
19. Knight OJ, Girkin CA, Budenz DL, Durbin MK, Feuer WJ; for the Cirrus OCT Normative Database Study Group. Effect of race, age, and axial length on optic nerve head parameters and retinal nerve fiber layer thickness measured by Cirrus HD-OCT. *Arch Ophthalmol*. 2012;130:312–318.
20. Chauhan BC, Danthurebandara VM, Sharpe GP, et al. Bruch's membrane opening minimum rim width and retinal nerve fiber layer thickness in a normal white population. *Ophthalmology*. 2015;122:1786–1794.
21. Tun TA, Sun C-H, Basjarab M, et al. Determinants of optical coherence tomography-derived minimum neuroretinal rim width in a normal Chinese population. *Invest Ophthalmol Vis Sci*. 2015;56:3337–3344.
22. Ramrattan RS, Wolfs RC, Jonas JB, Hofman A, de Jong PT. Determinants of optic disc characteristics in a general population: The Rotterdam Study. *Ophthalmology*. 1999; 106:1588–1596.
23. Vernon SA, Hawker MJ, Ainsworth G, Hillman JG, Macnab HK, Dua HS. Laser scanning tomography of the optic nerve head in a normal elderly population: the Bridlington Eye Assessment Project. *Invest Ophthalmol Vis Sci*. 2005;46:2823–2828.
24. Jonas JB. Optic disc size correlated with refractive error. *Am J Ophthalmol*. 2005;139:346–348.
25. Wang W, Xu L, Zhang L, Yang H, Ma Y, Jonas JB. Optic disc size in a population based study in northern China: the Beijing Eye Study. *Br J Ophthalmol*. 2006;90:353–356.
26. Xu L, Wang Y, Yang H, Zhang L, Jonas JB. Size of the neuroretinal rim and optic cup and their correlations with ocular and general parameters in adult Chinese: The Beijing Eye Study. *Br J Ophthalmol*. 2007;91:1616–1619.
27. Bourne RR, Foster PJ, Bunce C, et al. The morphology of the optic nerve head in the Shingaporean Chinese population (the Tanjong Pagar study): part 1—optic nerve head morphology. *Br J Ophthalmol*. 2008;92:303–309.
28. Bourne RR, Foster PJ, Bunce C, et al. The morphology of the optic nerve head in the Singaporean Chinese population (the Tanjong Pagar study): part 2—biometric and systemic associations. *Br J Ophthalmol*. 2008;92:310–314.
29. Nangia V, Matin A, Bhojwani Kulkarni M, Yadv M, Jonas JB. Optic disc size in a populatoin-based study in central India: the Central India Eye and Medical Study (CIEMS). *Acta Ophthalmol*. 2008;86:103–104.
30. Abe H, Shirakashi M, Tsutsumi T, et al.; for the Tajimi Study Group. Laser scanning tomography of optic discs of the normal Japanese population in a population-based setting. *Ophthalmology*. 2009;116:223–230.
31. Cheung CY, Chen D, Wong TY, et al. Determinants of quantitative optic nerve measurements using spectral domain optical coherence tomography in a population-based sample of non-glaucomatous subjects. *Invest Ophthalmol Vis Sci*. 2011;52:9629–9635.
32. Wu R-Y, Wong T-Y, Zheng Y-F, et al. Influence of refractive error on optic disc topographic parameters: the Singapore Malay Eye Study. *Am J Ophthalmol*. 2011;152:81–86.

33. Wu R-Y, Zheng Y-F, Wong T-Y, et al. Relationship of central corneal thickness with optic disc parameters: The Singpore Malay Eye Study. *Invest Ophthalmol Vis Sci*. 2011;52:1320–1324.
34. Tsutsumi T, Tomidokoro A, Araie M, Iwase A, Sakai H, Sawaguchi S. Planimetrically determined vertical cup/disc and rim width/disc diameter ratios and related factors. *Invest Ophthalmol Vis Sci*. 2012;53:1332–1340.
35. Budenz DL, Anderson DR, Varma R, et al. Determinants of normal retinal nerve fiber layer thickness measured by Stratus OCT. *Ophthalmology*. 2007;114:1046–1052.
36. Hirasawa H, Tomidokoro A, Araie M, et al. Peripapillary retinal nerve fiber layer thickness determined by spectral-domain optical coherence tomography in ophthalmologically normal eyes. *Arch Ophthalmol*. 2010;128:1420–1426.
37. Ooto S, Hangai M, Tomidokoro A, et al. Effects of age, sex, and axial length on the three-dimensional profile of normal macular layer structures. *Invest Ophthalmol Vis Sci*. 2011;52:8769–8779.
38. Mwanza JC, Durbin MK, Budenz DL, et al. Profile and predictors of normal ganglion cell-inner plexiform layer thickness measure with frequency-domain optical coherence tomography. *Invest Ophthalmol Vis Sci*. 2011;52:7872–7879.
39. Takayama A, Kita Y, Kita R, Tomita G. Influence of axial length on ganglion cell complex (GCC) thickness and on GCC thickness to retinal thickness ratios in young adults. *Jpn J Ophthalmol*. 2014;58:86–93.
40. Ikuno Y, Maruko I, Yasuno Y, et al. Reproducibility of retinal and choroidal thickness measurements in enhanced depth imaging and high-penetration optical coherence tomography. *Invest Ophthalmol Vis Sci*. 2011;52:5536–5540.
41. Garway-Heath DF, Poinooswamy D, Fitzke FW, Hitchings RA. Mapping the visual field to the optic disc in normal tension glaucoma eyes. *Ophthalmology*. 2000;107:1809–1815.
42. Bixenman WW, von Noorden GK. Apparent foveal displacement in normal subjects in cyclotropia. *Ophthalmology*. 1982;89:58–62.
43. Dieterich M, Brandt T. Ocular torsion and tilt of subjective visual vertical are sensitive brainstem signs. *Ann Neurol*. 1993;33:292–299.
44. Oohria A. Aging and objective physiologic excyclotorsion determined by fundus photography. *Nippon Ganka Gakkai Zasshi (J Jpn Ophthalmol Soc)*. 2016;120:548–551.
45. Jonas RA, Wang YX, Yang H, et al. Optic disc-fovea angle: The Beijing Eye Study 2011. *PLoS One*. 2011;10:e0141771.
46. Fortune B, Hardin C, Reynaud J, et al. Comparing optic nerve head rim width, rim area, and peripapillary nerve fiber layer thickness to axon count in experimental glaucoma. *Invest Ophthalmol Vis Sci*. 2016;57:OCT404–OCT412.
47. Clark RA, Demer JL. Effect of aging on human rectus extraocular muscle paths demonstrated by magnetic resonance imaging. *Am J Ophthalmol*. 2002;134:872–878.
48. Chaudhuri Z, Demer JL. Sagging eye syndrome. Connective tissue involution as a cause of horizontal and vertical strabismus. *JAMA Ophthalmol*. 2013;131:619–625.

Appendix A

The equation used for linear mixed effect model analysis was as follows:

$$\begin{aligned}\mathrm{BMO-MRW_{i,j}}\left(\mathrm{RNFLT_{i,j}}\right) = {} & \mathrm{A_{1,\,i}} + \mathrm{A_{2,\,i}} \times \mathrm{Sex_j} + \mathrm{A_{3,\,i}} \times \mathrm{Age_j} \\ & + \mathrm{A_{4,\,i}} \times \mathrm{AL_j} + \mathrm{A_{5,\,i}} \times \mathrm{CCT_j} \\ & + \mathrm{A_{6,\,i}} \times \mathrm{IOP_j} + \mathrm{A_{7,\,i}BMO_j} + \mathrm{b_j} \\ & + \mathrm{Error_{i,j}},\end{aligned}$$

where $\mathrm{BMO\text{-}MRW_{i,j}}$ ($\mathrm{RNFLT_{i,j}}$) indicates Bruch's membrane opening–minimum rim width (retinal nerve fiber layer thickness) in the i-th sector of the j-th subject; $\mathrm{Sex_j}$, $\mathrm{Age_j}$, $\mathrm{AL_j}$, $\mathrm{CCT_j}$, $\mathrm{IOP_j}$, and $\mathrm{BMO_j}$ indicate sex, age, axial length, central corneal thickness, intraocular pressure, and BMO area of the j-th subject eye; $\mathrm{b_j}$ represents random effect specific to the j-th subject eye; $\mathrm{A_{1,i}}$, an intercept for the i-th sector; $\mathrm{A_{2,i}}$ ($\mathrm{A_{3,i}}$,$\mathrm{A_{4,i}}$, $\mathrm{A_{5,i}}$, $\mathrm{A_{6,i}}$, $\mathrm{A_{7,i}}$) are coefficients of sex (age, AL, CCT, IOP, BMO area) for the BMO-MRW (RNFLT) in the i-th sector, with i = 1, 2, …., 6, and with j = 1, 2, 3, …, 258 in case of BMO-MRW and j = 1, 2, 3, …., 243 in case of RNFLT, respectively. $\mathrm{Sex_j}$ is equal to 1 (0), when the j-th subject is female (male). The first (second, third, fourth, fifth, and sixth) sector corresponds to the T, ST, IT, SN, IN, and N sector, respectively. $\mathrm{Error_{i,j}}$ represents error term in linear mixed model, and $\mathrm{b_j}$ and $\mathrm{Error_{i,j}}$ are independently distributed random variables following Gaussian distribution.

Appendix B

Table A1. Results of Linear Mixed Effect Model Analysis for BMO-MRW

Coefficient	Estimated Coefficient Value	*P* Value*
$\mathrm{A_{2,i}}$ effect of sex, female	3.60 ± 7.42† ~ 15.06 ± 7.42	>0.256
$\mathrm{A_{3,1}}$, effect of age on T sector	−0.76 ± 0.20	0.001
$\mathrm{A_{3,2}}$, effect of age on ST sector	−0.99 ± 0.20	<0.001
$\mathrm{A_{3,3}}$, effect of age on IT sector	−1.05 ± 0.20	<0.001
$\mathrm{A_{3,4}}$, effect of age on SN sector	−1.24 ± 0.20	<0.001
$\mathrm{A_{3,5}}$, effect of age on IN sector	−1.07 ± 0.20	<0.001
$\mathrm{A_{3,6}}$, effect of age on N sector	−1.14 ± 0.20	<0.001
$\mathrm{A_{4,i}}$ effect of AL	1.13 ± 3.97 ~ −5.27 ± 3.97	>0.500
$\mathrm{A_{5,i}}$, effect of CCT	0.01 ± 0.10 ~ −0.11 ± 0.10	>0.500
$\mathrm{A_{6,i}}$, effect of IOP	0.38 ± 1.55 ~ −3.56 ± 1.55	>0.131
$\mathrm{A_{7,1}}$, effect of BMO on T sector	−16.04 ± 7.69‡	0.224§
$\mathrm{A_{7,2}}$, effect of BMO on ST sector	−20.62 ± 7.69‡	0.045
$\mathrm{A_{7,3}}$, effect of BMO on IT sector	−27.88 ± 7.69	0.002
$\mathrm{A_{7,4}}$, effect of BMO on SN sector	−55.51 ± 7.69‡	<0.001
$\mathrm{A_{7,5}}$, effect of BMO on IN sector	−29.74 ± 7.69	<0.001
$\mathrm{A_{7,6}}$, effect of BMO on N sector	−39.32 ± 7.69	<0.001

i = 1, 2, 3, 4, 5, and 6 correspond to T, ST, IT, SN, IN, and N sector, respectively. AL, axial length (mm); BMO, Bruch's membrane opening area ($\mathrm{mm^2}$); BMO-MRW, Bruch's membrane opening–minimum rim width (μm); CCT, central corneal thickness (μm); IN, inferonasal; IOP, intraocular pressure (mm Hg); IT, inferotemporal; N nasal; SN, superonasal; ST, superotemporal; T, temporal.

* *P* values after Bonferroni's correction for multiple comparison.

† Standard error of estimate.

‡ Estimated coefficient value for the SN sector was more negative than that for the T and ST sectors ($P \leq 0.021$ after Bonferroni's correction).

§ $P = 0.037$ without Bonferroni's correction.

Appendix C

Table A2. Results of Linear Mixed Effect Model Analysis for RNFLT

Coefficient	Estimated Coefficient	*P* Value*
$A_{2,i}$, effect of sex, female	0.70 ± 2.68† ~ 5.80 ± 2.68	>0.185
$A_{3,1}$, effect of age on T sector	−0.05 ± 0.08‡	>0.500
$A_{3,2}$, effect of age on ST sector	−0.15 ± 0.08	0.322
$A_{3,3}$, effect of age on IT sector	−0.28 ± 0.08‡	0.001
$A_{3,4}$, effect of age on SN sector	−0.37 ± 0.08‡	<0.001
$A_{3,5}$, effect of age on IN sector	−0.24 ± 0.08	0.008
$A_{3,6}$, effect of age on N sector	−0.05 ± 0.08‡	>0.500
$A_{4,i}$, effect of AL§	2.10 ± 1.44 ~ −2.44 ± 1.44	>0.500
$A_{4,4}$, effect of AL on SN sector	−4.61 ± 1.44	0.009
$A_{5,i}$, effect of CCT	−0.01 ± 0.04 ~ −0.05 ± 0.04	>0.500
$A_{6,i}$, effect of IOP	0.20 ± 0.55 ~ −1.39 ± 0.55	>0.074
$A_{7,1}$, effect of BMO on T sector	5.11 ± 2.84	0.432
$A_{7,2}$, effect of BMO on ST sector	13.69 ± 2.84	< 0.001
$A_{7,3}$, effect of BMO on IT sector	8.18 ± 2.84	0.024
$A_{7,4}$, effect of BMO on SN sector	5.46 ± 2.84	0.327
$A_{7,5}$, effect of BMO on IN sector	13.51 ± 2.84	<0.001
$A_{7,6}$, effect of BMO on N sector	8.12 ± 2.84	0.026

i = 1, 2, 3, 4, 5, and 6 correspond to T, ST, IT, SN, IN, and N sector, respectively. RNFLT is measured along a circle with 3.5-mm-diameter centered on Bruch's membrane opening center (μm). AL, axial length (mm); BMO, Bruch's membrane opening area (mm^2); CCT, central corneal thickness (μm); IN, inferonasal; IOP, intraocular pressure (mm Hg); IT, inferotemporal; N, nasal; RNFLT, retinal nerve fiber layer thickness; SN, superonasal; ST, superotemporal; T, temporal.

* *P* values after Bonferroni's correction.

† Standard error of estimate.

‡ Estimated coefficient values for the T and S sectors were more positive than those for the IT and SN sectors ($P \leq 0.032$ after Bonferroni's correction).

§ i = 1, 2, 3, 4, 5, 6. Effect of axial length was significant only in the SN sector.

Investigative Ophthalmology & Visual Science